Pulsar Timing for the Fermi Gamma-ray Space Telescope

D. A. Smith, L. Guillemot, F. Camilo, Ismaël Cognard, D. Dumora, C. Espinoza, P. C. C. Freire, E. V. Gotthelf, A. K. Harding, G. B. Hobbs, et al.

Astronomy & Astrophysics

Pulsar timing for the *Fermi* gamma-ray space telescope[*]

D. A. Smith[1,2], L. Guillemot[1,2], F. Camilo[3], I. Cognard[4,5], D. Dumora[1,2], C. Espinoza[7], P. C. C. Freire[8], E. V. Gotthelf[3], A. K. Harding[9], G. B. Hobbs[10], S. Johnston[10], V. M. Kaspi[11], M. Kramer[7], M. A. Livingstone[11], A. G. Lyne[7], R. N. Manchester[10], F. E. Marshall[9], M. A. McLaughlin[12], A. Noutsos[7], S. M. Ransom[13], M. S. E. Roberts[14], R. W. Romani[15], B. W. Stappers[7], G. Theureau[4,5,6], D. J. Thompson[9], S. E. Thorsett[16], N. Wang[17], and P. Weltevrede[10]

[1] Université de Bordeaux, Centre d'études nucléaires de Bordeaux Gradignan, UMR 5797, 33175 Gradignan, France
  e-mail: smith@cenbg.in2p3.fr
[2] CNRS/IN2P3, Centre d'études nucléaires de Bordeaux Gradignan, UMR 5797, 33175 Gradignan, France
[3] Columbia Astrophysics Laboratory, Columbia University, New York, NY 10027, USA
[4] Laboratoire de Physique et Chimie de l'Environnement, LPCE UMR 6115, CNRS/INSU, 45071 Orléans, France
[5] Station de radioastronomie de Nançay, Observatoire de Paris, CNRS/INSU, 18330 Nançay, France
[6] GEPI, Observatoire de Paris, CNRS, Université Paris Diderot, Place Jules Janssen 92190 Meudon, France
[7] University of Manchester, Jodrell Bank Observatory, Macclesfield, Cheshire SK11 9DL, UK
[8] Arecibo Observatory, HC 3 Box 53995, Arecibo, Puerto Rico 00612, USA
[9] NASA Goddard Space Flight Center, Greenbelt, MD 20771, USA
[10] Australia Telescope National Facility, CSIRO, PO Box 76, Epping NSW 1710, Australia
[11] McGill University, Montreal, Quebec, Canada
[12] West Virginia University, Department of Physics, PO Box 6315, Morgantown, WV 26506, USA
[13] National Radio Astronomy Observatory, Charlottesville, VA 22903, USA
[14] Eureka Scientific, Inc., 2452 Delmer Street Suite 100, Oakland, CA 94602-3017, USA
[15] Department of Physics, Stanford University, California, USA
[16] Department of Astronomy & Astrophysics, University of California, Santa Cruz, CA 95064, USA
[17] National Astronomical Observatories-CAS, 40-5 South Beijing Road, Urumqi 830011, PR China

ABSTRACT

We describe a comprehensive pulsar monitoring campaign for the Large Area Telescope (LAT) on the *Fermi Gamma-ray Space Telescope* (formerly GLAST). The detection and study of pulsars in gamma rays give insights into the populations of neutron stars and supernova rates in the Galaxy, into particle acceleration mechanisms in neutron star magnetospheres, and into the "engines" driving pulsar wind nebulae. LAT's unprecedented sensitivity between 20 MeV and 300 GeV together with its 2.4 sr field-of-view makes detection of many gamma-ray pulsars likely, justifying the monitoring of over two hundred pulsars with large spin-down powers. To search for gamma-ray pulsations from most of these pulsars requires a set of phase-connected timing solutions spanning a year or more to properly align the sparse photon arrival times. We describe the choice of pulsars and the instruments involved in the campaign. Attention is paid to verifications of the LAT pulsar software, using for example giant radio pulses from the Crab and from PSR B1937+21 recorded at Nançay, and using X-ray data on PSR J0218+4232 from XMM-Newton. We demonstrate accuracy of the pulsar phase calculations at the microsecond level.

Key words. space vehicles: instruments – stars: pulsars: general – gamma-rays: observations – ephemerides

1. Introduction

Forty years after the discovery of rotating neutron stars much is unknown about their emission processes, and in particular the radio emission mechanism is still largely not understood (Lorimer & Kramer 2004; Lyubarsky 2008). Of the nearly two thousand known pulsars, six have been detected in GeV gamma-rays with high confidence, using the EGRET detector on the *Compton Gamma-Ray Observatory* (CGRO) (Thompson et al. 1999).

The Large Area Telescope (LAT) on the *Fermi* Gamma-ray Space Telescope (formerly the *Gamma-ray Large Area Space Telescope*, or GLAST) went into orbit on 2008 June 11 (Atwood et al. 2008). The sensitivity and time resolution of this instrument will allow it to discover tens or more of new gamma-ray pulsars (Smith & Thompson 2008). Notably, it will be able to determine the sources among the 169 unidentified EGRET sources that are pulsars. However, even with a sensitivity more than 30 times greater than that of EGRET, the LAT's rate of gamma-ray photon detection will be small. For example, the Crab pulsar is the third brightest known gamma-ray pulsar, but will trigger the LAT only once every 500 revolutions of the neutron star (15 s), on average. While the Crab pulsar should be detected by the LAT with high confidence in less than a day, it will take years to detect pulsars near the sensitivity threshold, with days separating individual photon arrival times. A search for pulsations using gamma-ray data alone is quite difficult in these conditions (Atwood et al. 2006; Ransom 2007). Accurate knowledge of the rotation parameters increases LAT pulsed sensitivity. However, many neutron stars slow down irregularly, a phenomenon known as "timing noise", making it difficult to

extrapolate a pulsar's rotation frequency ν from one epoch to another. Consequently, in order to obtain the accurate ephemerides necessary for gamma-ray detection of pulsations, known pulsars must be observed regularly.

In anticipation of the *Fermi* launch, and mindful of the requirement for accurate, contemporaneous timing parameters in order to observe pulsars at gamma-ray energies, we began an extensive campaign of pulsar timing observations with the Parkes 64-m radio telescope in Australia (Manchester et al. 2001), the Lovell 76-m telescope at the Jodrell Bank observatory near Manchester, England (Morris et al. 2002), and the 94-m (equivalent) Nançay radio telescope near Orleans, France. The Parkes telescope is the only telescope in the campaign that observes sources south of $-39°$. Theureau et al. (2005) describes the 2002 FORT upgrade to the Nançay receiver, with the new BON pulsar backend described in Cognard & Theureau (2006) and Camilo et al. (2007). These observatories carry out observing programs in support of the *Fermi* mission and, between them, observe more than 200 pulsars with a large spin-down luminosity, $\dot{E}$, as described below, on a regular basis. In addition, about 10 pulsars with weak radio emission that are particularly strong candidates for gamma-ray emission are being observed periodically with the Green Bank radio telescope (GBT) and the Arecibo radio telescope. Four pulsars with no detectable radio emission are being observed with the Rossi X-ray Timing Explorer satellite (RXTE). The Urumqi Observatory (Wang et al. 2001) is using a 25 m antenna to monitor 38 of the brighter radio pulsars. The goal is to build a database of rotation parameters that will allow folding of the gamma-rays as they are accumulated over the 5 to 10 year lifetime of the LAT. This work is similar in spirit to what was done for CGRO (Arzoumanian et al. 1994; Johnston et al. 1995; D'Amico et al. 1996; Kaspi 1994).

2. Pulsars and the Large Area Telescope

The LAT is described by Atwood et al. (2008). In brief, gamma-rays convert to electron-positron pairs in tungsten foil interleaved with layers of silicon microstrip detectors in the tracker, yielding direction information. The particle cascade continues in the cesium iodide crystals of the calorimeter, providing energy information. Scintillators surrounding the tracker aid rejection of the charged cosmic ray background. The scintillators are segmented to reduce the "backsplash": a self-veto effect that reduced EGRET's sensitivity to high energy photons.

The LAT is a 4-by-4 array of detector "modules" covering an area of roughly 1.7 m on a side. It is sensitive to photons with energies between 20 MeV and 300 GeV, whereas EGRET's sensitivity fell off significantly above 10 GeV. After event reconstruction and background rejection, the effective area for gamma-rays above 1 GeV is >8000 cm^2 at normal incidence, as compared to 1200 cm^2 for EGRET. The angular resolution is also better than EGRET's, such that source localisation for typical sources will be of order of $0.1°$ [1]. The height-to-width aspect ratio of the LAT is 0.4, for a field-of-view of 2.5 sr, or nearly 20% of the sky at a given time. Combined with the large effective area, this makes a sky survey observation strategy possible: on a given orbit, the LAT will sweep the sky 35° away from the orbital plane, covering 75% of the sky. At the end of the orbit, *Fermi* will rock to 35° on the other side of the orbital plane, and continue to scan. Thus, the entire sky is covered with good uniformity every three hours,

and no time is lost to earth occultation. Survey mode, large effective area, and good localisation together give the LAT an overall steady point-source sensitivity 30 times better than EGRET's.

Gamma-ray events recorded with the LAT have timestamps that derive from a GPS clock on the *Fermi* satellite. Ground tests using cosmic ray muons demonstrated that the LAT measures event times with precision relative to UTC significantly better than a microsecond (Smith et al. 2006). On orbit, satellite telemetry indicates comparable accuracy. The contribution to the barycentered time resolution from uncertainty in the LAT's position is negligible.

The EGRET pulsars showed a variety of pulse profiles and emission spectra and raised as many questions as they answered (Thompson 2004). The high-energy emission is thought to arise from basic electromagnetic interactions of highly relativistic particles, namely synchrotron emission, curvature emission and inverse Compton emission. In the two main categories of models describing high-energy emission by pulsars, charged particles are accelerated along the magnetic dipole field lines by parallel electric fields. The "polar cap" model (Ruderman & Sutherland 1975; Sturrock 1971) argues that the acceleration begins above the stellar magnetic pole, but can extend to the outer magnetosphere. In the "outer gap" model (Cheng et al. 1986a,b) particles are thought to be accelerated to high energies only in the outer magnetosphere, in vacuum gaps between a null-charge surface and the light cylinder.

The models predict different high-energy emission features such as spectra and profiles, that LAT observations may elucidate, through a hierarchy of observables. First, the different models have very different predictions of which and how many pulsars emit gamma-rays. Along with detections of radio-quiet pulsars in gamma-rays using blind search techniques, the LAT analysis using this timing program will constrain the ratio of radio-loud to radio-quiet pulsars. This ratio is different for the two emission models, with outer gap models predicting a much lower ratio (Gonthier et al. 2004; Harding et al. 2007). Reliable flux upper limits in the absence of gamma-ray pulsations are useful in this context (Nel et al. 1996) and also require good timing solutions.

The second observable is the emission profile. Its shape, as the beam sweeps the Earth, provides a cross-section of the regions in the pulsar magnetosphere where the emission originates. Coupled with radio intensity and polarization profile studies, as well as absolute phase, the gamma-ray light curve provides information on the emission geometry, which differs significantly from one model to another (Chiang & Romani 1994; Gonthier et al. 2002). The EGRET pulsars typically have two peaks, with the first one slightly offset in phase relative to the single radio peak. Although the Crab pulsar breaks this trend, LAT observations will study the prevalence of this behaviour as a function of pulsar age or other parameters. Pulsar detections and emission profiles can only be achieved through solid knowledge of the pulsar's rotation and good absolute time precision. The timing precision will allow finely binned profiles over many years even for millisecond pulsars.

The large energy range covered by the LAT will enable measurements of pulsar spectral cut-offs. Although EGRET observed high-energy cut-offs in pulsar spectra around a few GeV, it did not have the sensitivity to measure the exact energy or shape of the turnovers. For instance, the LAT should provide a determination of the Crab pulsar's spectral cut-off energy, known only to be less than a few tens of GeV (de Naurois et al. 2002; Teshima 2008), where EGRET lost sensitivity due to the backsplash effect. The on-axis LAT energy resolution is better

---

[1] Details of the instrument response are maintained at
http://www-glast.slac.stanford.edu/software/IS/
glast_lat_performance.htm

than 15% above 100 MeV and is better than 10% in the range between roughly 500 MeV and 50 GeV, and improves somewhat off-axis. The LAT should quickly measure the shape of the Vela pulsar spectral cut-off expected to be around 4 GeV, a powerful discriminator between polar cap and outer gap models and a potential diagnostic of high-energy emission altitude (Harding 2007). Finally, a subset of the pulsars detected by the LAT will have sufficient photon numbers to allow phase-resolved spectroscopy, offering further insight into emission mechanisms and the beam geometry.

The LAT will monitor all pulsars continuously with a duty-cycle of roughly one-sixth, because of its survey mode, unlike EGRET or the *Astro-rivelatore Gamma a Immagini LEggero* (AGILE) telescope (Pellizzoni et al. 2004), which went into orbit in April, 2007. A drawback of the survey strategy is that having the sample of gamma-photons spread over a longer duration makes phase-folding more difficult, as long-term timing noise may appear in pulsar spin behavior and glitches may occur (Ransom 2007). The need for a substantial and sustained pulsar timing campaign stems in part from this continuous observation, whereas pointing telescopes only require monitoring during observations of any given sky region.

3. The timing campaign

3.1. Possible gamma-ray pulsars

For a pulsar with a rotation frequency ν (s^{-1}) and frequency derivative $\dot{\nu} = \frac{d\nu}{dt}$ (in units of s^{-2}), the spin-down power is $\dot{E} = -4\pi^2 I \nu \dot{\nu}$ erg/s where the moment of inertia I is taken to be 10^{45} g cm^2. The open field-line voltage is $V \simeq 6.3 \times 10^{20} \sqrt{-\nu\dot{\nu}} \simeq 3.18 \times 10^{-3} \sqrt{\dot{E}}$ volts. Above some value of V, or, equivalently, $\dot{E}$, gamma-ray emitting electron-positron cascades occur, with gamma-ray luminosity L_γ increasing with $\dot{E}$ (Arons 1996). A linear dependence of L_γ on V would give $L_\gamma \propto -\nu^{0.5}\dot{\nu}^{0.5} \propto \sqrt{\dot{E}}$, leading to a gamma-ray production efficiency $\epsilon_\gamma = L_\gamma/\dot{E} \propto 1/\sqrt{\dot{E}}$. Analyses based on EGRET pulsar detections and upper limits have constrained gamma-ray luminosity laws (e.g. McLaughlin & Cordes 2000), an update of which yields $L_\gamma \propto\sim -\nu^{-0.9}\dot{\nu}^{0.6}$. Empirically, although based on a small handful of gamma-ray pulsars, the minimum spin-down threshold seems to be near $\dot{E} \simeq 3 \times 10^{34}$ erg/s (Thompson et al. 1999). The angular size and viewing geometry of pulsar beams is difficult to constrain and introduces a large uncertainty in the relation between a minimum $\dot{E}$ and the expected gamma-ray flux. Bright radio pulsars may have gamma-ray beams missing the Earth's line-of-sight; conversely at least one bright gamma-ray pulsar, Geminga, has no detectable radio flux (Burderi et al. 1999). Balancing these issues, and keeping the list of gamma-ray pulsar candidates of reasonable length, we have selected pulsars with $\dot{E} > 10^{34}$ erg/s for LAT pulsar timing. From the ATNF online catalogue (Manchester et al. 2005) we obtain 230 such pulsars. We give lower priority to the timing of the pulsars in globular clusters since they can have apparent $\dot{E}$ values higher than the true spin-down power of the neutron star, due to acceleration in the gravitational potential of the cluster. (Notable exceptions to this are the millisecond pulsars PSR B1820 − 30A and PSR B1821 − 24.) This leaves us with 224 pulsars which we believe are imperative to time regularly.

Table 1 gives the pulsar names as well as some indicators of whether they may be gamma-ray emitters, such as $\dot{E}$ and

associations with other high-energy sources[2]. The distance d is taken from the ATNF database (the variable "DIST1"). It is generally based on the NE2001 model for the Galactic distribution of free electrons (Cordes & Lazio 2002) but uses other information such as parallax or HI absorption measurements if they are available. The uncertainty in the derived distances can exceed 50%, depending on the pulsar. The table is sorted by decreasing $\sqrt{\dot{E}}/d^2$, assuming that $L_\gamma \propto V$ as discussed above. Such a ranking ignores effects of beam geometry relative to the Earth line-of-sight, and variations in L_γ that may stem from, for example, the angle between the neutron star's rotation and magnetic axes. Figure 1 shows $\sqrt{\dot{E}}/d^2$ normalized to Vela's value versus the rotation period for the large $\dot{E}$ pulsars.

Table 1 also lists some pulsar wind nebulae (PWN) associated with young pulsars (Kaspi et al. 2006; Roberts 2004). Of the many striking results recently obtained from the HESS atmospheric Cherenkov imager array is the large number of Galactic sources in the TeV sky, many of which have been identified as PWN (see for example Aharonian et al. 2006). Table 1 gives TeV associations with HESS sources as well as a MILAGRO source (Abdo et al. 2007). Some of the unidentified EGRET sources are also likely to be PWN or pulsars. The table includes the angular distances to nearby EGRET 3rd catalog sources (Hartman et al. 1999). Many young pulsars are in or near the error boxes for these sources, and the LAT will better localize the GeV sources, making coincidence tests stronger. The pulsar timing campaign will enhance searches for GeV pulsations, to address whether the origin is in the neutron star magnetosphere or in the nebula. One study aimed at distinguishing between true and fortuitous associations between young pulsars and their PWN or EGRET counterparts predicted that 19 ± 6 of the EGRET-pulsar proposed associations will be confirmed by the *Fermi* LAT observations (Kramer et al. 2003).

The table further lists those rare pulsars seen beyond radio wavelengths, either in optical ("O" in the table), or in X-rays. The larger gamma-ray pulsar sample expected from the LAT will improve the current poor knowledge of the correlations between different types of high-energy emission.

Although we base the LAT timing campaign on high $\dot{E}$ pulsars, we realize that pulsar gamma-ray emission is far from understood and therefore intend to study as many different pulsars as possible. The LAT's sensitivity and the continual sky-survey mode favor unexpected discoveries. The LAT team therefore welcomes long-term, phase-connected rotational ephemerides from astronomers wishing to collaborate on pulsed gamma-ray searches.

3.2. Timing radio-loud gamma-ray candidates

The radio telescope time needed to monitor a given pulsar depends on the precision needed by the LAT, its radio flux density (e.g. S_{1400} in the ATNF catalog) and pulse profile, and the magnitude of its timing noise. Simple simulations indicate that Gaussian smearing of gamma-ray arrival times barely degrades detection sensitivity, for smearing widths up to 0.05 periods. Once detected, gamma-photon statistics drive the need for higher precision: the timing residuals should be smaller than the phase histogram bin width, which in turn should be wide enough to have at least several gamma-photons per bin.

A consequence of these relatively modest timing requirements is that a given radio observation need only

---

[2] An up-to-date version is at https://confluence.slac.stanford.edu/display/GLAMCOG/Pulsars+being+timed

Table 1. Pulsars being timed for the Fermi Large Area Telescope (all known pulsars with $\dot{E} > 10^{34}$ erg/s), ordered by $\sqrt{\dot{E}}/d^2$, where $\dot{E}$ is the spin-down energy loss rate and d is the distance. $\sqrt{\dot{E}}/d^2$ as an indicator of expected gamma flux suffers many large uncertainties (see text). S_{1400} and S_{400} are the radio flux intensities at 1400 MHz and 400 MHz, respectively. "Cluster, Galaxy" is the name of the globular cluster or the host galaxy, if the pulsar is in one. "np" means that the source is observed in X-rays, but not pulsed. If the pulsar is located less than 2° away from a 3rd EGRET catalog source (Hartman et al. 1999), the EGRET name and the angular distance are listed. The asterisk (*) indicates that the 3EG source has more than one possible counterpart in the table. The TeV associations are taken from Wagner (2008), available at http://www.mpi-hd.mpg.de/hfm/HESS/public/HESS_catalog.htm, and from MILAGRO: (Abdo et al. 2007). Nearby pulsar wind nebulae (PWN) are noted in the last column (Kaspi et al. 2006; Roberts 2004). The data in the first 8 columns were obtained from the ATNF database except for the radio flux densities with the superscripts [a] Camilo, private communication, [b] Jacoby et al. (2003), [c] Kaspi et al. (1998), [d] Ray et al. (1996), [e] D'Amico et al. (2001), [f] Camilo et al. (2000). The full table is only available in electronic form at the CDS.

| PSR	PSRJ	$\frac{\sqrt{\dot{E}}}{d^2}$ % of Vela	$\dot{E}$ (erg/s)	d (kpc)	S_{1400} (mJy)	S_{400} (mJy)	Cluster, Galaxy	Optical X-ray	EGRET Nearby	EgretDist (°)	TeV assoc.	Notes
B0833−45	J0835−4510	100.	6.9e+36	0.3	1100.	5000.		OX	3EG J0834−4511	0.34	Vela	G263.9−3.3, Vela X
J0633+1746	J0633+1746	22.	3.3e+34	0.2	–	–		OX	3EG J0633+1751	0.24		G195.1+4.3, Geminga
B0531+21	J0534+2200	17.	4.6e+38	2.0	14.	646.		OX	3EG J0534+2200	0.13	Crab	G184.6−5.8, Crab, SN1054
J0437−4715	J0437−4715	14.	1.2e+34	0.2	142.	550.		X				G253.4−42.0
B0656+14	J0659+1414	7.42	3.8e+34	0.3	3.70	6.50		OX				Monogem Ring
B0743−53	J0745−5353	5.37	1.1e+34	0.2	–	23.						
J0034−0534	J0034−0534	1.90	3.0e+34	0.5	0.61	17.						
J0205+6449	J0205+6449	1.62	2.7e+37	3.2	0.04	–		X				G130.7+3.1, 3C 58, SN1181
J0613−0200	J0613−0200	1.58	1.3e+34	0.5	1.40	21.						
J1747−2958	J1747−2958	1.25	2.5e+36	2.0	0.07[a]	–			3EG J1744−3011 (*)	0.84	HESS J1745−303	G359.23−0.82, Mouse
B1706−44	J1709−4429	1.11	3.4e+36	2.3	7.30	25.		X	3EG J1710−4439	0.18		G343.1−2.3
B1055−52	J1057−5226	1.06	3.0e+34	0.7	–	80.		X	3EG J1058−5234	0.12		
J1740+1000	J1740+1000	0.99	2.3e+35	1.2	9.20	3.10						
B1951+32	J1952+3252	0.98	3.7e+36	2.5	1.00	7.00						G69.0+2.7, CTB 80
J1357−6429	J1357−6429	0.90	3.1e+36	2.5	0.44	–		X				
J1833−1034	J1833−1034	0.84	3.4e+37	4.7	0.07	–					HESS J1833−105	G21.5−0.9
B1509−58	J1513−5908	0.76	1.8e+37	4.2	0.94	1.50		X			HESS J1514−591	G320.4−1.2, MSH 15-52
B1257+12	J1300+1240	0.74	1.9e+34	0.8	2.00	20.		np				
J1524−5625	J1524−5625	0.73	3.2e+36	2.8	0.83	–						
J1531−5610	J1531−5610	0.69	9.1e+35	2.1	0.60	–						
B1046−58	J1048−5832	0.60	2.0e+36	2.7	6.50	–			3EG J1048−5840	0.14		G287.4+0.58
B0355+54	J0358+5413	0.56	4.5e+34	1.1	23.	46.						
J0940−5428	J0940−5428	0.50	1.9e+36	3.0	0.66	–						
J1930+1852	J1930+1852	0.44	1.2e+37	5.0	0.06	–		X	3EG J1928+1733	1.46		G54.1+0.3
B1259−63	J1302−6350	0.37	8.2e+35	2.8	1.70	–		np			HESS J1302−638	
J0834−4159	J0834−4159	0.36	9.9e+34	1.7	0.19	–						
J1909−3744	J1909−3744	0.36	2.2e+34	1.1	–	3.[b]						
B0906−49	J0908−4913	0.35	4.9e+35	2.5	10.	28.						G270.3−1.0
J1509−5850	J1509−5850	0.34	5.2e+35	2.6	0.15	–						
B1823−13	J1826−1334	0.34	2.8e+36	3.9	2.10	–		np	3EG J1826−1302 (*)	0.55	HESS J1825−137	G18.0−0.7
J1809−1917	J1809−1917	0.34	1.8e+36	3.5	2.50	–		np			HESS J1809−193	
J0538+2817	J0538+2817	0.32	4.9e+34	1.5	1.90	8.20		X				S147
J1811−1925	J1811−1925	0.32	6.4e+36	5.0	–	–		X			HESS J1809−193	G11.2−0.3, SN 386
J1420−6048	J1420−6048	0.31	1.0e+37	5.6	0.90	–		X	3EG J1420−6038	0.17	HESS J1420−607	G313.6+0.3, Kookaburra
B1800−21	J1803−2137	0.31	2.2e+36	3.9	7.60	23.		np			HESS J1804−216	
J1046+0304	J1046+0304	0.30	1.4e+34	1.1	0.30	–						
B0114+58	J0117+5914	0.30	2.2e+35	2.2	0.30	7.60						
J2229+6114	J2229+6114	0.28	2.2e+37	7.2	0.25	–		X	3EG J2227+6122	0.54		G106.6+3.1
J1718−3825	J1718−3825	0.28	1.2e+36	3.6	1.30	–			3EG J1714−3857	1.18	HESS J1718−385	
B1727−33	J1730−3350	0.27	1.2e+36	3.5	3.20	9.20			3EG J1734−3232	1.57		
B0740−28	J0742−2822	0.27	1.4e+35	2.1	15.	296.						
J1617−5055	J1617−5055	0.27	1.6e+37	6.8	0.5[c]	–		X			HESS J1616−508	
J1843−1113	J1843−1113	0.27	6.0e+34	1.7	0.10	–						
J2129−5721	J2129−5721	0.26	2.3e+34	1.4	1.40	14.						
J1124−5916	J1124−5916	0.26	1.2e+37	6.5	0.08	–		X				G292.0+1.8, MSH 11−54
J1846−0258	J1846−0258	0.25	8.1e+36	6.0	–	–		X			HESS J1846−029	G29.7−0.3, Kes 75
J1913+1011	J1913+1011	0.24	2.9e+36	4.8	0.50	–					HESS J1912+101	
J1911−1114	J1911−1114	0.23	1.2e+34	1.2	0.50	31.			3EG J1904−1124	1.96		
J2043+2740	J2043+2740	0.23	5.6e+34	1.8	–	15.[d]		X				
J0855−4644	J0855−4644	0.22	1.1e+36	3.9	0.20	–						
J0218+4232	J0218+4232	0.22	2.4e+35	2.7	0.90	35.		X	3EG J0222+4253	1.03		
J1739−3023	J1739−3023	0.20	3.0e+35	2.9	1.00	–			3EG J1744−3011 (*)	1.10		
J1831−0952	J1831−0952	0.20	1.1e+36	4.0	0.33	–						
B1957+20	J1959+2048	0.20	1.6e+35	2.5	0.40	20.		np				G59.2−4.7
J1105−6107	J1105−6107	0.20	2.5e+36	5.0	0.75	–		np	3EG J1102−6103	0.86		MSH 11−62
B1821−24	J1824−2452	0.19	2.2e+36	4.9	0.18	40.	M 28	X				
B1853+01	J1856+0113	0.19	4.3e+35	3.3	0.19	3.40			3EG J1856+0114	0.05		G34.7−0.4, W44, 3C 392
B1757−24	J1801−2451	0.18	2.6e+36	5.2	0.85	7.80		np	3EG J1800−2338	1.26		G5.27−0.9, G5.4-1.2?
B0611+22	J0614+2229	0.18	6.2e+34	2.1	2.20	29.			3EG J0617+2238	0.69		
B1719−37	J1722−3712	0.16	3.3e+34	1.9	3.20	25.						
J1835−1106	J1835−1106	0.16	1.8e+35	2.8	2.20	30.						
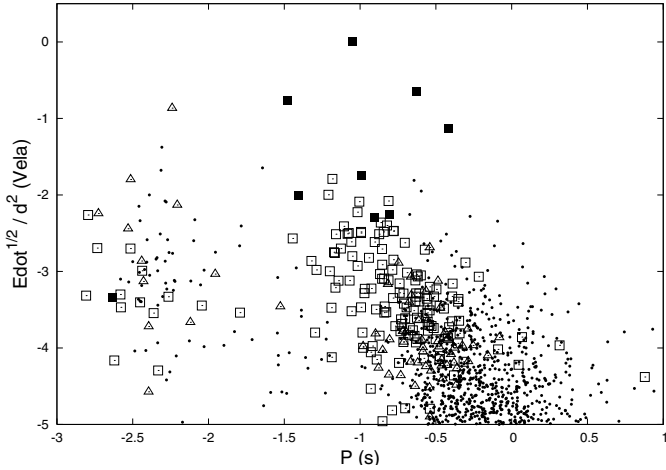
Fig. 1. $\sqrt{\dot{E}}/d^2$, normalized to Vela, versus neutron star rotation period. The pulsars with $\dot{E} > 3 \times 10^{34}$ erg/s (squares) and with 10^{34} erg/s $< \dot{E} < 3 \times 10^{34}$ erg/s (triangles) are those being timed regularly for the Large Area Telescope. The 9 solid squares correspond to the six confirmed EGRET pulsed detections and three pulsars for which there were indications of gamma-ray pulsations. Dots: other pulsars. Pulsars in globular clusters are not plotted. Note that radio pulsars with high $\sqrt{\dot{E}}/d^2$ may nevertheless have gamma-ray beams directed away from the Earth line-of-sight and escape detection.

Fig. 2. Timing residuals for the 3.05 ms pulsar B1821−24, observed with the Nançay radio telescope using a constant dispersion measure. Crosses: 1.4 GHz, Squares: 2 GHz. Adding a dispersion measure time derivative to the fit aligns the residuals for the two frequencies.

last the minimum time for detection. More crucial is the number of observations per year, which depends on the timing noise, correlated with ν and $\dot{\nu}$ and thus $\dot{E}$ (Arzoumanian et al. 1994; Cordes & Helfand 1980). Gamma-ray candidates tend to be the noisiest pulsars. Illustrations of timing noise in young, high $\dot{E}$ pulsars can be found, e.g., in Hobbs et al. (2006a). Glitches have been observed for roughly a quarter of the pulsars being monitored (Melatos et al. 2008). The bulk of the pulsars in this campaign are observed monthly, and a smaller number are observed weekly or bi-weekly.

The low radio fluxes of some gamma-ray pulsar candidates require long exposures on the biggest radio telescopes. We must devote time to these as they could be bright gamma-ray sources. Radio-faint, particularly noisy pulsars could dominate the observation schedules.

Radio signals are dispersed by the interstellar medium, with a frequency dependent delay causing signals at high radio frequencies to arrive before those at low radio frequencies. The pulsar Dispersion Measure (DM), or the integrated column density of free electrons along the line of sight from a pulsar to Earth, usually measured in cm^{-3} pc, allows extrapolation of the photon arrival times from radio to infinite frequency, as is required for gamma-ray studies. The DM, however, can change over timescales of weeks to years (You et al. 2007). If the DM is inaccurate, then the reference phase Φ_0 from the radio ephemeris (described below) will change, causing an apparent drift in the gamma-ray absolute phase and a smearing of the resulting gamma-ray pulse profiles. Such smearing would compromise the multi-wavelength phase comparisons upon which beam geometry studies are based. Therefore the timing campaign must include occasional monitoring at multiple radio frequencies. Figure 2 is one illustration of the magnitude of the dispersion for different radio frequencies.

Another illustration of the potential effect of DM changes on a gamma-ray light curve is obtained using the DM values from the Jodrell Bank monthly Crab ephemerides. Over the years of the Compton GRO mission (1991–1999), the maximum
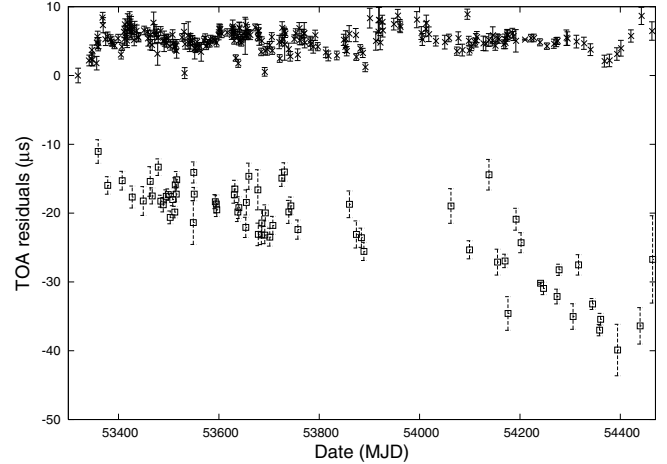
excursion in the photon time extrapolated from the radio frequency of 1400 MHz to infinite frequency is 0.3 ms (1% of a rotation of the neutron star). For reference, the total DM correction from radio to gamma ray is ~120 ms, which is 4 Crab rotations. For pulsars faster than the Crab, the effect could be larger. For most pulsars, the effect is minor. Turbulence in the interstellar medium also induces frequency-dependent scattering and refraction of the pulsar signal, due to path-length differences. Simulations show that those effects are in the order of hundreds of nanoseconds for observations at 1.4 GHz (Foster & Cordes 1990), and hence negligible for gamma-ray astronomy.

The radio pulsar monitoring must be sustained throughout the duration of the *Fermi* mission (i.e. for 5 to 10 years), a strain for any observatory, so other contributions are welcome. In particular, very frequent monitoring of high $\dot{E}$, large S_{1400} pulsars could allow significant contributions to LAT science by smaller radio telescopes.

3.3. Radio-quiet and radio-faint pulsars

The archetypical radio-quiet gamma-ray pulsar is Geminga, PSR J0633+1746. Biannual XMM satellite measurements have ensured maintenance of a phase-coherent set of rotation parameters over the last few years (Jackson & Halpern 2005). The LAT will measure accurate light curves for Geminga in a few days and will maintain an accurate ephemeris through gamma-ray timing. The AGILE gamma-ray telescope has recently detected Geminga (Pellizzoni, private communication).

Table 1 includes at least 15 other pulsars outside of globular clusters with $S_{1400} \leq 0.1$ mJy (some of the others without listed S_{1400} values are also faint), requiring long radio telescope integration times, if detectable at all. 10 of these have $\dot{E} > 10^{36}$ erg/s, making them both especially promising gamma-ray candidates, and subject to especially large timing noise.

Four high $\dot{E}$ pulsars are being timed with the Rossi X-ray Timing Explorer satellite (RXTE: PSR J1811−1925 in the center of the supernova remnant G11.2−0.3; the young pulsar J1846−0258 in the core of a Crab-like pulsar wind nebula at the center of the bright shell-type SNR Kes 75, possibly the youngest known rotation-powered pulsar (Livingstone et al. 2006); and B0540−69 and J0537−6910 in the Large Magellanic Cloud.

The remaining six high $\dot{E}$, low S_{1400} pulsars are J0205+6449, J1124−5916, J1747−2958, J1833−1034, J1930+1852, and J2021+3651. Depending on the pulse shape and the intensity of the surrounding radio nebulae, some of these are detectable with the 70-m class telescopes. For the others, the Arecibo and Green Bank (GBT) radio telescopes are more appropriate.

LAT will also perform "blind" searches for new radio-quiet pulsars (Ziegler et al. 2008), that is, search for pulsations in gamma-ray sources which are not known pulsars. Furthermore, the LAT may detect gamma-ray sources bearing neutron star signatures, for which no pulsations are observed, as was the case for the EGRET source 3EG J1835+5918 (Reimer et al. 2001; Halpern et al. 2007). The positional uncertainty obtained with the LAT should be small enough so that Arecibo, GBT and Parkes can perform deep radio pulsation searches.

3.4. Public access to data

All public data are released through the Fermi Science Support Center (FSSC). The details and schedule for the LAT data releases can be found at http://fermi.gsfc.nasa.gov/ssc/data/policy/. During the first year of operations, which will be devoted primarily to an all-sky survey, summary information about a variety of variable sources will be released. At the end of this period, all LAT photon data and associated science analysis tools will be released; thereafter, photon data will be released as soon as processed, typically within days of detection.

As LAT gamma-ray results are published, the ephemerides used will be posted on the FSSC server in a "D4 FITS" file (described below). An effort will be made to publish a large fraction of the timing solutions acquired in this campaign around the end of the first year. In any case, the first-year timing solutions for all 224 pulsars will be made public 6 months after the end of year 1. Users will be asked to cite the timing parameter creators in publications, or to work with them directly. The intent is to update a large number of high $\dot{E}$ pulsar rotation ephemerides in the years following, but the continuation of the timing campaign will depend on the results of Cycle 1.

It is hoped that the pulsar timing data will also be used to analyse data from instruments other than the LAT. Atmospheric Cherenkov telescopes and neutrino detectors are just two examples of experiments that could benefit from the timing campaign. Researchers wanting pulsar timing data may contact the authors.

4. *Fermi* LAT analysis software

4.1. The "Science Tools" and the ephemerides database

The *Fermi* LAT "Science Tools" provide a framework for analyzing gamma-ray data recorded by the Large Area Telescope: data selection, exposure calculation, source detection and identification, likelihood analysis of emission spectra, etc.[3]. The "Science Tools" are developed and maintained by the FSSC and instrument teams. This software is based on the standard *ftools* developed at HEASARC[4], designed for data sets using the FITS format. In this section we describe *gtbary* and *gtpphase*, which are pulsar timing analysis tools.

---

[3] http://fermi.gsfc.nasa.gov/ssc/data/analysis/SAE_overview.html
[4] http://heasarc.gsfc.nasa.gov/lheasoft/ftools/ftools_menu.html

The pulsar section of the "Science Tools" allows basic timing analyses within the FSSC framework, but is *not* intended to replace specialized packages such as *TEMPO* (Taylor & Weisberg 1989) or *TEMPO2* (Hobbs et al. 2006b). The pulsar science tools include only a subset of the functions provided by the those packages.

We have tested *gtbary* and *gtpphase* with giant radio pulses from the Crab pulsar (B0531+21) and from the millisecond pulsar B1937+21, recorded at the Nançay radio telescope, X-ray photons from the binary millisecond pulsar J0218+4232 recorded by XMM, as well as with simulated radio observations of the binary millisecond pulsar J0437−4715 from Parkes.

Furthermore, we made extensive use of pulsar timing solutions (ephemerides) obtained from radio or X-ray pulsar observations. We converted ephemerides to fit the LAT format, a FITS file called "D4", which contains a subset of the many parameters that pulsar astronomers provide. The web interface to the ephemerides database generates the D4 FITS file needed by the Science Tools.

When doing a long-term follow-up of a pulsar, one might have to use overlapping ephemerides, or choose between ephemerides valid on the same epoch. Those ephemerides could come from different observatories possibly using different analysis methods. As an example, the definition of the arbitrary time T_0 when the pulsar rotational phase equals zero, i.e. $\Phi(T_0) = 0$ can differ between observatories. To ensure phase continuity when using overlapping pulsar timing solutions, it is important to have the template profiles used to build the ephemerides. The web-based tool will keep track of these template profiles. In the following we describe the pulsar timing analysis using the LAT software, and the different tests used to validate this process.

4.2. Building light curves with LAT software

Topocentric photon arrival times recorded at the observatory at finite frequency have to be transfered to solar system barycenter (SSB) times at infinite frequency, mainly by correcting times for the motion of the earth and the observatory in the solar system frame. Then one folds the barycenter times, using the truncated Taylor series expansion for $\Phi(t)$:

$$\Phi(t) = \Phi_0 + \sum_{i=0}^{i=N} \frac{f_i \times (t - T_0)^{i+1}}{(i+1)!} \tag{1}$$

where T_0 is the reference epoch of the pulsar ephemeris, f_i is the frequency derivative of order i, and Φ_0 is the absolute phase, an arbitrary pulsar phase at $t = T_0$.

We have tested both *barycenter* and *phase-folding* tools. The procedure is:

– conversion of the arrival times from the observatory-specific format to the LAT time format: Mission Elapsed Time (MET) TT, which is the number of seconds since 2001 January 1 at 00:00 (UTC);
– calculation of the orbital or ground-based observatory position, and conversion to the LAT spacecraft position format;
– transfer of the topocentric times to the barycentric frame, using *"gtbary"*;
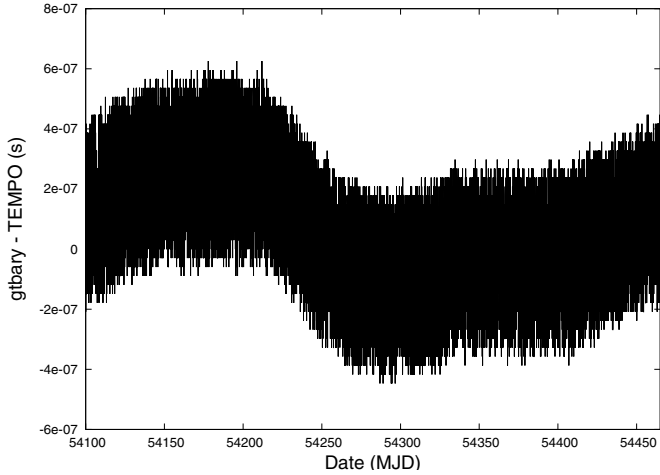– calculation of the pulsar phase for each arrival time, using *"gtpphase"*.

Fig. 3. *TEMPO-gtbary* comparison. *TEMPO2-gtbary* looks very similar.

4.3. Simulated observations of an artificial pulsar

To test the barycenter software alone, we have simulated arrival times at Nançay observatory and compared LAT barycenter software with *TEMPO* and *TEMPO2*.

Some time and coordinate definition differences exist between these different codes. Most *TEMPO* pulsar timing solutions have been published using the JPL DE200 planetary ephemerides (Standish 1990). *TEMPO* forms barycentric times in "Barycentric Dynamic Time" (TDB). *TEMPO2* uses the JPL DE405 (Standish 1998) solar system ephemerides and computes barycentric time in "Barycentric Coordinate Time" (TCB) units, taking into account the time dilation results from Irwin & Fukushima (1999). The LAT barycenter tool *gtbary* handles both the DE200 ephemerides and the recommended DE405 model, also forming TDB times. The relation between TDB and TCB times is given by:

$$\text{TDB} \simeq \text{TCB} - L_B \times \Delta T \qquad (2)$$

where $L_B = 1.550519767 \times 10^{-8} \pm 2 \times 10^{-17}$ and $\Delta T =$ (date − 1977 January 1, 00:00) TAI×86 400 s. TAI times refer to "International Atomic Time". (*TEMPO2* has a *TEMPO* emulation mode, setting the barycentric time to TDB.) More details on time-coordinate definitions can be found in Andersen (1999), Rickman (2001) and McCarthy & Petit (2004).

In the simulation, 10 000 arrival times are recorded on the ground, beginning on MJD 54 100 (arbitrary), with a constant step size (no assumption of periodic emission is made), over 1 year. Nançay times are expressed in Modified Julian Days (MJD) UTC, at finite frequency. They first have to be moved to the LAT time format, at infinite frequency. The dispersion delay in the propagation of a signal at a frequency at the solar system barycenter f_{SSB} through the interstellar medium is the following:

$$\Delta t = -\frac{DM}{K f_{\text{SSB}}^2} \qquad (3)$$

where $K \equiv 2.410 \times 10^{-4} \text{ MHz}^{-2} \text{ cm}^{-3} \text{ pc s}^{-1}$ is the *dispersion constant* (see e.g. Manchester & Taylor 1977) and *DM* is the dispersion measure. Note that the frequency at the barycenter f_{SSB} is different from the frequency at the observatory, due to the Doppler shift resulting from the motion of the observatory with respect to the pulsar (Edwards et al. 2006). Higher order relativistic corrections are neglected here. The simulated values for
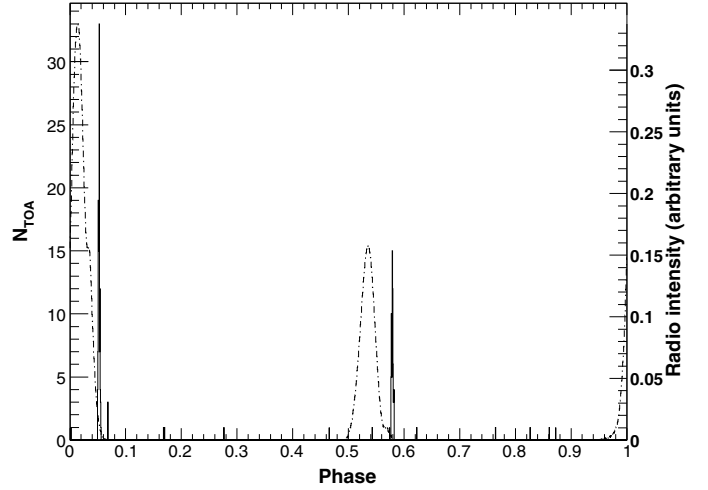

Fig. 4. Giant radio pulses from B1937+21 recorded at Nançay (solid line, left-hand scale). The ~2 μs pulse width reflects the accuracy of the phase-folding. Also shown is the template radio profile at 1.4 GHz used for this study (dashed line, right-hand scale).

the pulsar position at J2000 epoch and dispersion measure are $(\alpha, \delta) = (20.75°, 45°)$, and $DM = 0$ cm^{-3} pc.

The position of the radio telescope with respect to the solar system barycenter for each time of arrival was calculated using the DE200 model in the *TEMPO-gtbary* comparison, and using the DE405 model with *TEMPO2* in TDB mode for the *TEMPO2-gtbary* comparison. The topocentric times are then transfered to the SSB. The resulting differences as a function of time are shown in Fig. 3. In both cases, time differences are below 0.7 μs, better than the instrumental precision. We conclude that there is agreement between the LAT barycenter code and the other standard tools.

4.4. Giant radio pulses from the Crab pulsar and B1937+21, recorded at Nançay

Giant pulses are known only from a handful of young and millisecond pulsars, and occupy very small windows of pulsar phase (see e.g. Johnston & Romani 2004; Knight et al. 2006). Times of arrival for 3498 main component Crab GRPs with signal to noise ratio exceeding 20 standard deviations were recorded over eight months with the Nançay radio telescope, as described in Oosterbroek et al. (2008). The radio data were de-dispersed after detection and times and observatory positions for each date are converted to the LAT format. Data were folded using contemporaneous Jodrell Bank ephemerides (Lyne et al. 1993), with accuracy better than 160 μs. Event times were then converted to the barycenter using *gtbary* and phase-folded with *gtpphase*. The mean GRP arrival time is 32 μs before that predicted by the Jodrell Bank ephemerides, well within ephemeris accuracies. The null phase shift of the GRPs relative to the predicted phase is consistent with the results of Shearer et al. (2003). This demonstrates our ability to phase gamma-ray data over many months, even in the presence of significant timing noise, validating the codes to a few tens of μs.

Giant pulses from B1937+21 were originally discovered and studied in detail by Cognard et al. (1996). A study by Kinkhabwala & Thorsett (2000) revealed that they occur in windows shorter than 10 μs, 55 to 70 μs after the main radio pulse and interpulse, allowing us to probe shorter timescales. Dates for 251 giant radio pulses with signal to noise exceeding 30 standard
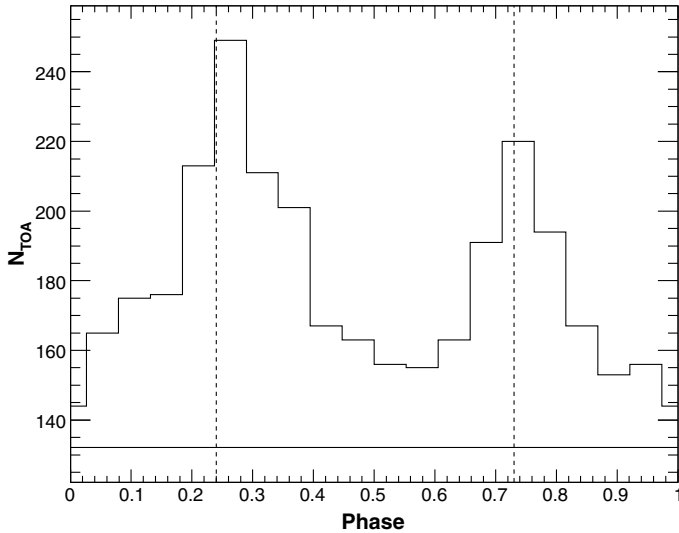
Fig. 5. X-ray photons from J0218+4232, recorded by the XMM-Newton satellite, between 1.6 and 4 keV. Black solid line: mean background level. Black dotted lines: peak positions in Webb et al. (2004), respectively $\Phi_1 = 0.24$ and $\Phi_2 = 0.73$.
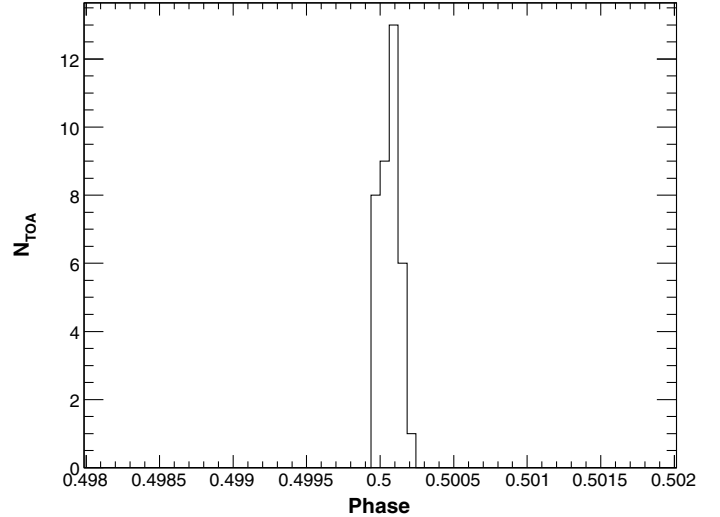

Fig. 6. Simulated times of arrival from the binary millisecond pulsar J0437−4715 recorded at Parkes. The absolute phase is defined so that the main radio pulse is centered on 0.5.

deviations were recorded with the Nançay radio telescope over three weeks. The timing solution was derived from Nançay data. We phase-folded event times having corrected the pulsar position for proper motion. Figure 4 shows the resulting phases, along with a pulse profile at 1.4 GHz. The mean delays between the main and secondary giant pulse components and their regular emission counterparts are 60.1 and 67.3 μs respectively, with rms deviations of 1.9 and 2.4 μs, consistent with Kinkhabwala & Thorsett's results. The narrow pulse widths demonstrate our precision to a few μs, albeit for a more stable system over a shorter duration.

4.5. X-ray data from PSR J0218+4232, observed by XMM-Newton

Orbital movement has to be taken into account for pulsars in binary systems. The 2.3 millisecond pulsar J0218+4232 is in a binary system with a low mass white dwarf (Kuiper et al. 2002). It has been extensively studied at gamma-ray energies and is expected to be a bright *Fermi* source (Guillemot et al. 2007).

XMM-Newton, an X-ray satellite operating between 0.1 and 12 keV, made a 36 ks observation of J0218+4232 on 2002 February 11–12, with the PN camera[5]. In timing mode, this instrument has a timing resolution of 30 μs. Only events well calibrated in energy were retained. Pulsar data were collected using a rectangular region centered on the source. The background level (shown in Fig. 5) was estimated by selecting data from a similar region, in the same dataset, centered about 50″ away from the pulsar, where no X-ray source could be detected. Finally, only events with energy between 1.6 and 4 keV were selected, to allow comparison with studies using the same dataset done by Webb et al. (2004).

Event times recorded by XMM-Newton are expressed in MET TT since 1998 January 1 at 00:00 (TT), and hence have to be converted to the LAT time format. As for the standard XMM-Newton analysis, satellite positions as a function of time were determined by a combination of Kepler orbital parameters

and Chebyshev polynomials. Positions were interpolated to fit the LAT position format.

Event times were converted to the barycenter, then corrected for the pulsar orbital motion and folded, based on radio ephemerides given in Kuiper et al. (2002). We tested frequencies around the nominal value with a χ^2 test, and found a shift in frequency of $\Delta \nu = 2.6 \times 10^{-6}$ Hz. As noted by Webb et al. (2004), who found a similar offset, such a shift is well within the resolution of the timing data. The resulting phase histogram between 1.6 and 4 keV is shown in Fig. 5. The peaks are centered on 0.26 and 0.74 respectively, which are within 40 μs of Webb et al's results.

4.6. Simulated radio data for PSR J0437−4715 observed with the Parkes telescope

The millisecond pulsar J0437−4715 has a pulse period of 5.76 ms, and is in a binary system with a 5.74 day orbital period. "Post-Keplerian" (PK) parameters, such as the rate of periastron advance, $\dot{\omega}$, or the rate of orbital period decay, $\dot{P}_b$, can be fit for this binary system (e.g. van Straten et al. 2001).

A 500 day observation of J0437−4715 at the Parkes observatory was simulated using *TEMPO2* with the *FAKE* plugin, generating 37 times of arrival. The simulation used a timing solution for J0437−4715 with 200 ns accuracy, derived from real Parkes observations from April 1996 to March 2006 (Verbiest et al. 2008). *TEMPO2* generated a *gtpphase*-compatible solution, since the LAT Science Tools allow fewer orbital parameters than *TEMPO2*. The accuracy of the simplified timing solution was 300 ns.

Event times were transfered to the solar system barycenter, having corrected for radio dispersion and pulsar proper motion. Times of arrival were phase-folded based on the *gtpphase*-compatible version of the J0437−4715 ephemeris, yielding the phase histogram in Fig. 6. The mean phase calculated with the LAT software is delayed from the *TEMPO2* mean value by 0.32 μs, resulting in a validation of the code below the μs level.

---

[5] We thank N. Webb (CESR – Toulouse) for providing us with the XMM-Newton data.

5. Conclusions

We have motivated and described the large timing campaign that is underway for the *Fermi* mission (formerly GLAST). Previous campaigns resulted in a wealth of information on young pulsars, and we expect this effort will expand gamma-ray pulsar detections to middle-aged, older and millisecond pulsars as well. A large database of gamma-ray pulsars of many types will allow a study of trends and correlations in important properties such as gamma-ray flux, spectral index, profile shape and spectral cutoff.

References

Abdo, A. A., Allen, B., Berley, D., et al. 2007, ApJ, 664, 91
Aharonian, F., Akhperjanian, A. G., Bazer-Bachi, A. R., et al. 2006, A&A, 460, 365
Andersen, J. 1999, Trans. IAU, Ser. B, 23
Arons, J. 1996, A&AS, 120, 49
Arzoumanian, Z., Nice, D. J., Taylor, J. H., & Thorsett, S. E. 1994, ApJ, 422, 671
Atwood, W. B., Ziegler, M., Johnson, R. P., & Baughman, B. M. 2006, ApJ, 652, 49
Atwood, W. B., et al. 2008, ApJ, submitted
Burderi, L., Fauci, F., & Boriakoff, V. 1999, ApJ, 512, 59
Camilo, F., Lorimer, D. R., Freire, P., Lyne, A. G., & Manchester, R. N. 2000, ApJ, 535, 975
Camilo, F., Cognard, I., Ransom, S. M., et al. 2007, ApJ, 663, 497
Cheng, K. S., Ho, C., & Ruderman, M. 1986a, ApJ, 300, 500
Cheng, K. S., Ho, C., & Ruderman, M. 1986b, ApJ, 300, 522
Chiang, J., & Romani, R. W. 1994, ApJ, 436, 754
Cognard, I., & Theureau, G. 2006, in On the Present and Future of Pulsar Astronomy, 26th meeting of the IAU, 2, 36
Cognard, I., Shrauner, J. A., Taylor, J. H., & Thorsett, S. E. 1996, ApJ, 457, 81
Cordes, J. M., & Helfand, D. J. 1980, ApJ, 239, 640
Cordes, J. M., & Lazio, T. J. W. 2002 [arXiv:astro-ph/0207156]
D'Amico, N., Grueff, G., Montebugnoli, S., et al. 1996, ApJS, 106, 611
D'Amico, N., Lyne, A. G., Manchester, R. N., Possenti, A., & Camilo, F. 2001, ApJ, 548, 171
de Naurois, M., Holder, J., Bazer-Bachi, R., et al. 2002, ApJ, 566, 343
Edwards, R. T., Hobbs, G. B., & Manchester, R. N. 2006, MNRAS, 372, 1549
Foster, R. S., & Cordes, J. M. 1990, ApJ, 364, 123
Gonthier, P. L., Ouellette, M. S., Berrier, J., O'Brien, S., & Harding, A. K. 2002, ApJ, 565, 482
Gonthier, P. L., Van Guilder, R., & Harding, A. K. 2004, ApJ, 604, 775
Guillemot, L., Lonjou, V., Dumora, D., et al. 2007, in AIP Conf. Ser., ed. S. Ritz, P. F. Michelson, & C. A. Meegan, 921, 395
Halpern, J. P., Camilo, F., & Gotthelf, E. V. 2007, ApJ, 668, 1154
Harding, A. K. 2007, AIP Conf. Ser. 921, ed. S. Ritz, P. F. Michelson, & C. A. Meegan, 49
Harding, A. K., Grenier, I. A., & Gonthier, P. L. 2007, Ap&SS, 309, 221
Hartman, R. C., Bertsch, D. L., Bloom, S. D., et al. 1999, ApJS, 123, 79
Hobbs, G. B., Edwards, R. T., & Manchester, R. N. 2006a, MNRAS, 369, 655
Hobbs, G. B., Lyne, A. G., & Kramer, M. 2006b, Chinese J. Astron. Astrophys. Suppl., 6, 169
Irwin, A. W., & Fukushima, T. 1999, A&A, 348, 642
Jackson, M. S., & Halpern, J. P. 2005, ApJ, 633, 1114
Jacoby, B. A., Bailes, M., van Kerkwijk, M. H., et al. 2003, ApJ, 599, 99

Johnston, S., & Romani, R. W. 2004, Young Neutron Stars and Their Environments, ed. F. Camilo, & B. M. Gaensler, IAU Symp., 218, 315
Johnston, S., Manchester, R. N., Lyne, A. G., Kaspi, V. M., & D'Amico, N. 1995, A&A, 293, 795
Kaspi, V. M. 1994, Ph.D. Thesis, Princeton University
Kaspi, V. M., Crawford, F., Manchester, R. N., et al. 1998, ApJ, 503, 161
Kaspi, V. M., Roberts, M. S. E., & Harding, A. K. 2006, Isolated neutron stars (Compact stellar X-ray sources), 279 [arXiv:astro-ph/0402136]
Kinkhabwala, A., & Thorsett, S. E. 2000, ApJ, 535, 365
Knight, H. S., Bailes, M., Manchester, R. N., Ord, S. M., & Jacoby, B. A. 2006, ApJ, 640, 941
Kramer, M., Bell, J. F., Manchester, R. N., et al. 2003, MNRAS, 342, 1299
Kuiper, L., Hermsen, W., Verbunt, F., et al. 2002, ApJ, 577, 917
Livingstone, M. A., Kaspi, V. M., Gotthelf, E. V., & Kuiper, L. 2006, ApJ, 647, 1286
Lorimer, D. R., & Kramer, M. 2004, Handbook of Pulsar Astronomy (Cambridge University Press)
Lyne, A. G., Pritchard, R. S., & Graham-Smith, F. 1993, MNRAS, 265, 1003, monthly Crab ephemerides at http://www.jb.man.ac.uk/pulsar/crab.html
Lyubarsky, Y. 2008, in 40 Years of Pulsars: Millisecond Pulsars, Magnetars and More, ed. C. Bassa, Z. Wang, A. Cumming, & V. M. Kaspi, AIP Conf. Ser., 983, 29
Manchester, R. N., & Taylor, J. H. 1977, Pulsars (W. H. Freeman), 36
Manchester, R. N., Lyne, A. G., Camilo, F., et al. 2001, MNRAS, 328, 17
Manchester, R. N., Hobbs, G. B., Teoh, A., & Hobbs, M. 2005, AJ, 129, 1993
McCarthy, D. D., & Petit, G. 2004, IERS Conventions (International Earth Rotation and Reference Systems Service (IERS))
McLaughlin, M. A., & Cordes, J. M. 2000, ApJ, 538, 818
Melatos, A., Peralta, C., & Wyithe, J. S. B. 2008, ApJ, 672, 1103
Morris, D. J., Hobbs, G., Lyne, A. G., et al. 2002, MNRAS, 335, 275
Nel, H. I., Arzoumanian, Z., Bailes, K. T. S., et al. 1996, A&AS, 120, 89
Oosterbroek, T., Cognard, I., Golden, A., et al. 2008, A&A, 488, 271
Pellizzoni, A., Chen, A., Conti, M., et al. 2004, Adv. Space Res., 33, 625
Ransom, S. M. 2007, in ed. S. Ritz, P. F. Michelson, & C. A. Meegan, AIP Conf. Ser., 921, 54
Ray, P. S., Thorsett, S. E., Jenet, F. A., et al. 1996, ApJ, 470, 1103
Reimer, O., Brazier, K. T. S., Carramiñana, A., et al. 2001, MNRAS, 324, 772
Rickman, H. 2001, Trans., IAU, Ser. B, 24
Roberts, M. S. E. 2004, The Pulsar Wind Nebula Catalog (March 2005 version), available at http://www.physics.mcgill.ca/~pulsar/pwncat.html
Ruderman, M. A., & Sutherland, P. G. 1975, ApJ, 196, 51
Shearer, A., Stappers, B., O'Connor, P., et al. 2003, Science, 301, 493
Smith, D. A., & Thompson, D. J. 2008, in Neutron stars and pulsars, 40 years after the discovery, ed. W. Becker, in press
Smith, D. A., Grove, J. E., Siskind, J. S., & Dumora, D. 2006, Muon Coincidence Absolute Timing Tests, Tech. Rep. LAT-TD-08777-03, Fermi mission
Standish, E. M. 1990, A&A, 233, 252
Standish, E. M. 1998, A&A, 336, 381
Sturrock, P. A. 1971, ApJ, 164, 529
Taylor, J. H., & Weisberg, J. M. 1989, ApJ, 345, 434
Teshima, M. 2008, The Astronomer's Telegram, 1491, 1
Theureau, G., Coudreau, N., Hallet, N., et al. 2005, A&A, 430, 373
Thompson, D. J. 2004, in Cosmic Gamma-Ray Sources, ed. K. S. Cheng, & G. E. Romero, Astrophysics and Space Science Library, 304, 149
Thompson, D. J., Bailes, M., Bertsch, D. L., et al. 1999, ApJ, 516, 297
van Straten, W., Bailes, M., Britton, M., et al. 2001, Nature, 412, 158
Verbiest, J. P. W., Bailes, M., van Straten, W., et al. 2008, ApJ, 679, 675
Wagner, R. 2008, available at http://www.mpi-hd.mpg.de/hfm/HESS/public/HESS_catalog.htm
Wang, N., Manchester, R. N., Zhang, J., et al. 2001, MNRAS, 328, 855
Webb, N. A., Olive, J.-F., & Barret, D. 2004, A&A, 417, 181
You, X. P., Hobbs, G. B., Coles, W. A., et al. 2007, MNRAS, 378, 493
Ziegler, M., Baughman, B. M., Johnson, R. P., & Atwood, W. B. 2008, ApJ, 680, 620